Paper No.
09256

NACE INTERNATIONAL CORROSION 2009 CONFERENCE & EXPO

CORROSION BEHAVIOR OF CARBON STEEL IN SUPERCRITICAL CO_2 – WATER ENVIRONMENTS

Yoon-Seok Choi and Srdjan Nešić
Institute for Corrosion and Multiphase Technology
Department of Chemical Engineering
Ohio University, Athens, OH 45701, USA

ABSTRACT

The corrosion behavior of carbon steel was investigated under supercritical CO_2 ($scCO_2$) – water systems to simulate the condition of CO_2 transportation pipeline in the CO_2 sequestration applications. To understand the thermodynamic properties of $scCO_2$-water systems related to the corrosion phenomena, thermodynamic modeling were conducted to determine the mutual solubilities of CO_2 and water in the two coexisting phases, and to calculate the concentrations of corrosive species in the free water at various pressures and temperatures. Carbon steel samples were exposed to water-saturated CO_2, and CO_2-saturated water in the pressure range of 40 to 80 bar at 50°C. The corrosion rate of samples was determined by weight loss measurements. The surface morphology and the composition of the corrosion product layers were analyzed by using surface analytical techniques (SEM and EDS).

Keywords: supercritical CO_2, thermodynamic modeling, CO_2 corrosion, carbon steel

INTRODUCTION

Emissions from fossil fuel-fired power plants represent a significant source of carbon dioxide (CO_2) emissions, a known greenhouse gas. The capture and storage of CO_2 in geological reservoirs is now considered to be one of the main options for achieving deep reductions in greenhouse gas emissions.[1,2] The CO_2 capture and storage process involves three stages: capture of the CO_2 from the power plant or industrial process, transmission of the CO_2 to the storage site followed by injection into the geological reservoir.[3] In order to avoid two-phase flow regimes and increase the density of the CO_2, the captured CO_2 gas is typically compressed to the supercritical state while the temperature and the pressure are over 31.1°C and 73.8 bar, respectively, thereby making it easier and less costly to transport.[3,4] The research activities are largely concentrating on development of the capture technology to reduce costs, and on assessing the technical feasibility of injecting and monitoring the CO_2

within the geological reservoirs themselves.[5] Little of the research is being conducted on CO_2 transmission, but this remains a critical component that should not be overlooked.

Low alloy carbon steel pipelines have been used for transportation of CO_2 at high pressure, but in all cases, CO_2 must be dried to eliminate the corrosion risk.[6] However, if CO_2 transport is to be achieved at a large scale or in existing pipelines, it will not be practical to dry it sufficiently and liquid water "breakout" is to be expected. Furthermore, drying CO_2 contributes to an increase in handling cost, especially for offshore installations where weight allowance and space for process equipment installation are very restricted.[7] When free water exists in the pipeline, it will be saturated with CO_2 and the corrosion rate will be significant for carbon steel because of the formation of carbonic acid (H_2CO_3). In addition, even though pure, dry supercritical CO_2 is not corrosive, there are several studies which provide qualitative evidence for corrosion on carbon steel in water-saturated supercritical CO_2 phase.[8,9] Thus, to be able to consider the corrosion risk in such pipelines, quantitative evaluation of corrosion in both CO_2-saturated water and water-saturated CO_2 phases will be needed.

The impact of CO_2 corrosion on carbon steel has been studied extensively at pressures relevant for oil and gas transport (up to 20 bar CO_2). At higher pressures experimental data are sparse. Since CO_2 changes from gaseous to liquid or supercritical with increasing pressure, it will lead to different interaction with water, i.e. CO_2 solubility in water will not follow Henry's law in liquid or supercritical CO_2 conditions, which results in changing water chemistry. Since the solubility of water in CO_2 is related to the free–liquid water formation and the solubility of CO_2 in water correlates with the corrosive potential of free water, accurate estimations of the mutual solubilities of CO_2 and water are important issue in the CO_2 transportation pipeline corrosion. Although many studies have been done to model mutual solubilities of CO_2 and water at high pressures, there is no attempt to predict the water chemistry at such a high pressure.

Thus, in the present study, to understand the thermodynamic properties of CO_2-water systems related to the corrosion phenomena, thermodynamic modeling were conducted to determine the mutual solubilities of CO_2 and water in the two coexisting phases, and to calculate the concentrations of corrosive species in the free–liquid water at various ranges of pressure and temperature (up to 300 bar, 85^{o}C). In addition, the corrosion properties with increasing pressure were investigated for carbon steel by weight loss measurements and surface analysis techniques.

THERMODYNAMIC MODELING

The thermodynamic model used in this work was based on a combination of Spycher model[10] (mutual solubilities of CO_2 and water) and Nesic model[11] (chemistry of water-rich phase).

Modeling for mutual solubilities of CO_2-water system

Spycher et al. reviewed the published experimental P-T-x data for CO_2-water system in the temperature range of 12~100^{o}C and pressure up to 600 bar to develop a solubility model.[10] They used non-iterative procedure to calculate the composition of the compressed CO_2 and liquid phase at equilibrium based on equating chemical potentials and using the Redlich-Kwong (RK) equation of state (EOS).[12] Their procedure is kept as simple as possible and is suitable for our purpose to establish a preliminary thermodynamic model to predict the mutual

solubilities of CO_2 and water in high pressure CO_2 pipeline applications. In the following, an approach for calculating the mutual solubilities of CO_2 and water is presented using the Spycher model.

At equilibrium of CO_2-water system, the following equilibrium relationship can be written:

$$H_2O_{(g)} \leftrightarrow H_2O_{(l)} \quad (1)$$

$$K_{H_2O} = f_{H_2O(g)}/a_{H_2O(l)} \quad (2)$$

$$CO_{2(g)} \leftrightarrow CO_{2(aq)} \quad (3)$$

$$K_{CO_2} = f_{CO_2(g)}/a_{CO_2(aq)} \quad (4)$$

where K is true equilibrium constants, f is fugacity of the gas components, and a is activity of components in the liquid phase. The K values for water and CO_2 are functions of pressure and temperature as:

$$K_{(T,P)} = K^0_{(T,P^0)} \exp\left(\frac{(P-P^0)\bar{V}_i}{RT}\right) \quad (5)$$

where P, P^0, R, T are pressure, reference pressure (1 bar), gas constant and temperature in K, respectively. $\bar{V}_i$ is the average partial molar volume of the pure component i over the pressure interval P^0 to P.

From the definition of fugacity ($f_i = \phi_i y_i P$)[13], the mole fraction of water in the CO_2 phase (y_{H_2O}) can be written with combining equation (2) and (5):

$$y_{H_2O} = \frac{K^0_{H_2O} a_{H_2O}}{\phi_{H_2O} P} \exp\left(\frac{(P-P^0)\bar{V}_{H_2O}}{RT}\right) \quad (6)$$

where, ϕ_{H_2O} is the fugacity coefficient of water.

For better accuracy at high pressures, the water activity deviation from unity caused by dissolved CO_2 should be taken into account. Using Raoult's law, the water activity can be approximated by its mole fraction in the water phase ($x_{H_2O} = 1 - x_{CO_2}$), such that:

$$y_{H_2O} = \frac{K^0_{H_2O}(1-x_{CO_2})}{\phi_{H_2O} P} \exp\left(\frac{(P-P^0)\bar{V}_{H_2O}}{RT}\right) \quad (7)$$

where, x_{CO_2} is the mole fraction of CO_2 in water phase. There is following relationship between a_{CO_2} and x_{CO_2}:

$$a_{CO_2} = 55.508 x_{CO_2} \quad (8)$$

Substituting equation (5) and (8) into equation (4) gives:

$$x_{CO_2} = \frac{\phi_{CO_2}(1-y_{H_2O})P}{55.508 K^0_{CO_2(g)}} \exp\left(-\frac{(P-P^0)\bar{V}_{CO_2}}{RT}\right) \quad (9)$$

Equations (7) and (9) can be solved directly by setting:

$$A=\frac{K^0_{H_2O}}{\phi_{H_2O}P_{tot}}\exp\left(\frac{(P-P^0)\bar{V}_{H_2O}}{RT}\right) \quad (10)$$

$$B=\frac{\phi_{CO_2}P_{tot}}{55.508K^0_{CO_2(g)}}\exp\left(-\frac{(P-P^0)\bar{V}_{CO_2}}{RT}\right) \quad (11)$$

Using parameters A and B, we can calculate the mole fraction of water in the CO_2 phase (y_{H_2O}) and the mole fraction of CO_2 in the water phase (x_{CO_2}) as follows:

$$y_{H_2O}=\frac{(1-B)}{\left(\frac{1}{A}-B\right)} \quad (12)$$

$$x_{CO_2}=B(1-y_{H_2O}) \quad (13)$$

The average partial molar volume of the pure water ($\bar{V}_{H_2O}$ = 18.1 cm^3/mol) and CO_2 ($\bar{V}_{CO_2(g)}$= 32.6 cm^3/mol, $\bar{V}_{CO_2(l)}$= 32 cm^3/mol), and the K parameters were obtained from the literature and/or by calibration to the solubility data:

$$\log K^0_{H_2O}=-2.209+3.097\times10^{-2}T-1.098\times10^{-4}T^2+2.048\times10^{-7}T^3 \quad (14)$$

$$\log K^0_{CO_2(g)}=1.189+1.304\times10^{-2}T-5.446\times10^{-5}T^2 \quad (15)$$

$$\log K^0_{CO_2(l)}=1.169+1.368\times10^{-2}T-5.380\times10^{-5}T^2 \quad (16)$$

where T is temperature in ^oC.

The fugacity coefficients in equations (10) and (11) should be derived from an equation of state (EOS) which can calculate properties of CO_2-water mixtures. In this study, Redlich-Kwong (RK) EOS was used to get the fugacity coefficients and the volume of the compressed gas phase. The RK EOS is given by[12]:

$$P=\left(\frac{RT}{V-b}\right)-\left(\frac{a}{T^{0.5}V(V+b)}\right) \quad (17)$$

where V is the molar volume of the CO_2-rich phase at pressure P and temperature T, and R is the gas constant. Parameters a and b characterize intermolecular attraction and repulsion, respectively.

For CO_2-water mixtures, the mixture constants a_{mix} and b_{mix} can be calculated by the standard mixing rules:

$$a_{mix}=\sum_{i=1}^{n}\sum_{j=1}^{n}y_iy_ja_{ij}=y^2_{H_2O}a_{H_2O}+2y_{H_2O}y_{CO_2}a_{H_2O\text{-}CO_2}+y^2_{CO_2}a_{CO_2} \quad (18)$$

$$b_{mix}=\sum_{i=1}^{n}y_ib_i=y_{H_2O}b_{H_2O}+y_{CO_2}b_{CO_2} \quad (19)$$

From these mixing rules and equation (17), the fugacity coefficient of component k in mixture with other component i can be calculated as:

$$\ln(\phi_k) = \ln\left(\frac{V}{V-b_{mix}}\right) + \left(\frac{b_k}{V-b_{mix}}\right) - \left(\frac{2\sum_{i=1}^{n} y_i a_{ik}}{RT^{1.5} b_{mix}}\right) \ln\left(\frac{V+b_{mix}}{V}\right) + \left(\frac{a_{mix} b_k}{RT^{1.5} b_{mix}^2}\right) \left[\ln\left(\frac{V+b_{mix}}{V}\right) - \left(\frac{b_{mix}}{V+b_{mix}}\right)\right] - \ln\left(\frac{PV}{RT}\right) \quad (20)$$

To avoid an iterative scheme, the assumption of infinite water dilution in the CO_2-rich phase is made that y_{H_2O}= 0 and y_{CO_2}=1 in the mixing rules in equation (18) and (19). Then, a_{mix} and b_{mix} can be replaced to a_{CO_2} and b_{CO_2} in equation (20), respectively. And the volume of the compressed gas phase (V) can be calculated by recasting RK EOS in terms of volume:

$$V^3 - V^2\left(\frac{RT}{P}\right) - V\left(\frac{RTb_{CO_2}}{P} - \frac{a_{CO_2}}{PT^{0.5}} + b_{CO_2}^2\right) - \left(\frac{a_{CO_2} b_{CO_2}}{PT^{0.5}}\right) = 0 \quad (21)$$

where, R=83.1447 barcm^{3}mol^{-1}K^{-1}, V is in cm^3/mol, P is in bar, and T is in K.

A FORTRAN program was used to calculate the mutual solubilities of CO_2 and water in the temperature range of 15~85^{o}C and pressure up to 300 bar.

Modeling for the chemistry of free water and for the prediction of $FeCO_3$ precipitation

Understanding water chemistry is an important precondition for predicting corrosion under high CO_2 pressure. The concentrations of carbonic species ($CO_{2(aq)}$, H_2CO_3, HCO_3^-, and CO_3^{2-}) as well as pH in the water phase were calculated to provide a tool for estimating water chemistry of a pipeline when water precipitates using the solubility of CO_2 and equilibrium constants for each chemical reaction at various pressure and temperature ranges. In the case of CO_2 transporting pipelines, due to a virtually unlimited supply of CO_2, there is constant partial pressure of CO_2 on the surface of free water so that the system can be considered as an 'open' system.

Once CO_2 dissolves in water (equation (3)), $CO_{2(aq)}$ is involved in a sequence of chemical reactions as follows:

$$CO_{2(aq)} + H_2O \overset{Khyd}{\longleftrightarrow} H_2CO_3 \quad \text{(Hydration of aqueous } CO_2\text{)} \quad (22)$$

$$H_2CO_3 \overset{Kca}{\leftrightarrow} H^+ + HCO_3^- \quad \text{(Dissociation of carbonic acid)} \quad (23)$$

$$HCO_3^- \overset{Kbi}{\leftrightarrow} H^+ + CO_3^{2-} \quad \text{(Dissociation of bicarbonate ion)} \quad (24)$$

$$H_2O \overset{Kw}{\leftrightarrow} H^+ + OH^- \quad \text{(Dissociation of water)} \quad (25)$$

With the partial pressure of CO_2 known in an open system, Henry's law can be applied in order to calculate the vapor-liquid equilibrium of CO_2 at low pressure.[14] However, at high pressure, Henry's law can't be used to calculate the concentration of CO_2 in the solution. Thus, in the present study, the concentrations of CO_2 in the water (C_{CO_2}) were calculated using the solubility of CO_2 in water (x_{CO_2}) obtained from equation (13).

Once concentration of dissolved CO_2 is fixed, the reactions shown above can be described by equilibria reactions as follows based on the assumption of infinite dilution:

$$K_{hyd} = \frac{C_{H_2CO_3}}{C_{CO_2} C_{H_2O}} \quad (26)$$

$$K_{ca} = \frac{C_{H^+} C_{HCO_3^-}}{C_{H_2CO_3}} \quad (27)$$

$$K_{bi} = \frac{C_{H^+} C_{CO_3^{2-}}}{C_{HCO_3^-}} \quad (28)$$

$$K_w = \frac{C_{H^+} C_{OH^-}}{C_{H_2O}} \quad (29)$$

where $C_{H_2CO_3}$, $C_{HCO_3^-}$, $C_{CO_3^{2-}}$, C_{H^+}, and C_{OH^-} are the concentrations (mol/L) of carbonic acid, bicarbonate ion, carbonate ion, hydrogen ion, and hydroxide ion, respectively.

The equilibrium constants, K, are a function of the temperature and are available in the open literature. Since the solution cannot have a net charge, an electroneutrality relation is required. Mathematically, it is expressed:

$$C_{H^+} = C_{HCO_3^-} + 2 \times C_{CO_3^{2-}} + C_{OH^-} \quad (30)$$

Supersaturation (SS) of iron carbonate is calculated using the following equation:[15,16]

$$SS = \frac{C_{Fe^{2+}} \cdot C_{CO_3^{2-}}}{K_{SP}} \quad (31)$$

where $C_{Fe^{2+}}$ is the concentration of ferrous ion in the solution, and K_{SP} is the solubility limit of iron carbonate. The scale will precipitate when the SS value exceeds unity i.e. when the solution is supersaturated. From the literature review, it is found that the Greenberg and Tomson equation[17] is the best choice for describing iron carbonate solubility limit as a function of temperature. It should be noted that Greenberg and Tomson's experiments used a de-ionized water solution and assumed that ionic strength is 0. However, it can be calculated that the ionic strength was actually 0.002 because of the other ions present in the solution, such as H^+, HCO_3^-, CO_3^{2-}, and OH^-, Fe^{2+}. When this is accounted for, a slightly revised equation is obtained:[15]

$$\log K_{sp} = -59.3498 - 0.041377 T_K - \frac{2.1963}{T_K} + 24.5724 \log(T_K) \quad (32)$$

A FORTRAN and excel programs were used to calculate the concentrations of species in the solution and the precipitation of iron carbonate with various temperature and pressure ranges.

EXPERIMENTAL PROCEDURE

The test specimens were machined from X65 low carbon steel with a size of 25 X 15 X 3 mm. The composition of this steel is given in Table 1. The specimens were ground with 600 grit silicon carbide paper, cleaned with alcohol in ultrasonic bath, dried, and weighed using a balance with a precision of 0.1 mg. The electrolyte used in this work was 1 wt.% NaCl solution.

The weight loss experiments were performed in a 2000 psi static autoclave with 1000 ml volume (Figure 1). 400 ml of solution was added to the autoclave and CO_2 gas was bubbled for 3 h to remove oxygen before starting the test. Corrosion tests were conducted under different pressures (40 ~ 80 bar) at 50^{o}C. When both water and CO_2 are added in the autoclave, there is a phase separation with the water phase at the bottom. Corrosion coupons were inserted both in the water-saturated CO_2 phase at the top of the autoclave and in the CO_2-saturated water phase at the bottom.

The corrosion rates were determined from weight-loss method at the end of a 24-hour exposure. The specimens were removed and cleaned for 5 min in the Clarke's solution (20 g antimony trioxide + 50 g stannous chloride and hydrochloric acid to make 1000 ml). The specimens were then rinsed in distilled water, dried and weighed to 0.1 mg. The corrosion rate can be calculated by the following equation[18]:

$$\text{Corrosion rate (mm/y)} = \frac{8.76\times10^{4}\times\text{weight loss (g)}}{\text{area (cm}^2)\times\text{density (g/cm}^3)\times\text{time (hour)}} \qquad (33)$$

The morphology and compositions of corrosion products were analyzed by SEM and EDS.

RESULTS

Thermodynamic modeling

The mutual solubilities of CO_2 and water calculated using equations (12) and (13) are shown in Figures 2 and 3 in terms of mole fractions of water and CO_2. The solubility of water in CO_2 showed high values at low pressures, passes through a minimum, and then increased with pressure. The discontinuity in water solubility at subcritical temperatures (15, 25^{o}C) coincides with the phase change from a gaseous to a liquid CO_2. Above the critical temperature (31.1^{o}C), it is related to the phase change from a gaseous to a supercritical CO_2 after which trend with pressure becomes smoother. However, the solubility of CO_2 in water increased sharply with rising pressure up to the saturation pressure and at a lesser rate thereafter. The CO_2 solubility trend with pressure reflected two solubility curves for two distinct phases: liquid or supercritical CO_2 above saturation pressure, and gaseous CO_2 below this pressure. This resulted in a break in slope on the overall solubility trends.

Furthermore, as shown in Figures 2 and 3, the CO_2-water system is highly asymmetric: solubility of water in CO_2 is smaller than that of CO_2 in water by one order of magnitude. This is due to the property difference of molecular CO_2 and water.[19] CO_2 is a non-polar molecule and the key intermolecular force is the London force, while water is a strong polar molecule and intermolecular interaction depends primarily on hydrogen bonds. In the CO_2-water binary mixture, molecular interactions between two like molecules are much stronger than those between two unlike molecules (water and CO_2). This dissimilarity results in the low solubility of water in the CO_2-rich phase. The electrostatic forces of water molecules can polarize CO_2 molecules, and then increase their ability to penetrate the water phase; consequently, the solubility of CO_2 in water is much larger than that of water in CO_2. Since the amount of water in CO_2 is quite small, such that the CO_2 properties (density, conductivity) can be approximated fairly well by those of pure CO_2.

The effects of temperature on the solubility of water and on the solubility of CO_2 are significantly different, and the solubility of water increased while the solubility of CO_2 decreased with increase in temperature. This behavior of the CO_2-water system is due probably to changes in compressibility of CO_2 and hydration of water[20]: e.g., at 80 bar the density of CO_2 is 707.2 kg/m^3 at T=30^{o}C and becomes 966 kg/m^3 at T=0^{o}C, indicating that the resistance for water to penetrate into CO_2 decreases with increase temperature; in comparison, water density varies with temperature only slightly, and the effect of hydration, which enhance the dissolution of CO_2 in water is greater at low temperature than at high temperatures.

Figure 4 shows a comparison between the predicted solubility of water in CO_2 and that from experimental data available in the literature.[21-26] The comparison demonstrates an acceptable match in the temperature range of 15~50^{o}C, however, calculated water solubility has less accurate at higher temperatures, because the water mole fractions in the CO_2 phase keeps increasing with temperature so that the assumption of infinite water dilution should eventually breakdown. A comparison between solubility of CO_2 in water calculated using the model versus the experimental data[21-26] is represented in Figure 5. Results presented in Figure 5 show a good agreement at various temperatures and pressures.

The effects of pressure and temperature on the concentrations of carbonic species (H_2CO_3, HCO_3^-, and CO_3^{2-}) and pH (H^+) are shown in Figures 6 and 7. The concentrations of H_2CO_3 and HCO_3^- showed a same trend as the solubility of CO_2 in water shown in Figure 3, i.e., the concentrations increased with increasing pressure whereas decreased with temperature. However, the concentration of CO_3^{2-} increased with increasing pressure and temperature. The pH value changed in the range of 4.4 to 3 which decreased with an increase in pressure and increased with increasing temperature. The pH of free water will be in the range of 3.1 ~ 3.3 under supercritical CO_2 condition (P>73 bar, T>31.1^{o}C), which can lead more acidic environment compare with atmospheric condition (pH 3.9 at 1 bar, 25^{o}C). At this low pH values, the solubility of iron carbonate is sufficiently high that no precipitate would be observed (scale-free CO_2 corrosion).

Corrosion tests under supercritical CO_2-water system

Figure 8 shows the corrosion rate of carbon steel under different pressures at 50^{o}C. Note that the CO_2 phase was gaseous at 40 and 60 bar, whereas it was supercritical at 80 bar. Corrosion coupons in the CO_2-rich phase did not show any visible corrosion attack, and low corrosion rates were measured. As shown in Figure 8, the corrosion rates in CO_2-saturated water phase are much higher than in water-saturated CO_2 phase. However, there is little difference in the corrosion rate with pressure in CO_2-saturated water phase. Based on the water chemistry predicted in Figure 7 (b), the pH in these experiments would be 3.25 (40 bar), 3.18 (60 bar), and 3.14 (80 bar), which suggests an iron carbonate scale-free CO_2 corrosion. At pH 4 or below, direct reduction of H^+ ions ($2H^+ + 2e^- \rightarrow H_2$) is important and the pH has a direct effect on the corrosion rate.[27] However, the most important effect of pH is indirect and relates to how pH changes conditions for formation of iron carbonate scales. High pH results in a decreased solubility of iron carbonate and leads to an increased precipitation rate and higher scaling tendency. To predict this, the degree of saturation for iron carbonate as a function of pressure at 50^{o}C with different ferrous ion concentrations and pH are shown in Figures 9 and 10. The ferrous ion concentrations were selected based on the results of the corrosion tests. It has been found that under test conditions (40 ~ 80 bar) iron carbonate is under-saturated

when pH is 3 and supersaturated when pH is 4 with more than 200 ppm of the ferrous ion concentration.

Figures 11 and 12 show the surface morphologies of the corroded samples at different pressures before and after cleaning with the Clarke's solution. The analysis by SEM and EDS revealed that the morphologies were almost identical with pressure, and the surface was locally covered by the corrosion products ($FeCO_3$). This indicates that iron dissolution reaction proceeds with time and leads to an increase in pH at the steel surface by accumulating dissolved ferrous ions, and then iron carbonate precipitate due to the local supersaturation.[28] However, as shown in Figure 8, corrosion rates did not change much with pressure, even if some iron carbonate precipitation occurs, reflecting the fact that a relatively porous, detached and unprotective scale was formed. In addition, after removing these corrosion products, a severe uniform corrosion attack for all samples was revealed (Figure 12).

CONCLUSIONS

The mutual solubilities of CO_2 and water, and the chemistry of the free water in a wide temperature and pressure ranges were predicted by thermodynamic modeling works. In addition, the corrosion properties with increasing pressure were investigated for carbon steel by weight loss measurements and surface analysis techniques. The following conclusions are drawn:

- The solubility of water in CO_2 and the solubility of CO_2 in water at supercritical CO_2 condition increased with increasing pressure, however, the solubility of CO_2 in water was much larger than that of water in CO_2.
- The solubility of water in CO_2 increased while the solubility of CO_2 in water decreased with increase in temperature.
- The calculated water solubility in CO_2 showed that the agreements between the calculation results and the experimental data were quite well at low and medium temperatures, and up to 300 bar of pressure. When temperature was above 75^{o}C, there were remarkable discrepancies.
- The calculated CO_2 solubility in water from 15 to 85^{o}C, and up to 300 bar showed a good agreement with experimental data.
- The concentrations of $CO_{2(aq)}$, H_2CO_3 and HCO_3^- increased with increasing pressure but decreased with an increase in temperature. The concentration of CO_3^{2-} increased linearly with increasing pressure and temperature, and the pH value changed in the range of 4.4 to 3 which decreased with an increase in pressure and increased with increasing temperature.
- Corrosion coupons in the CO_2-rich phase did not show any significant corrosion attack, and low corrosion rates were obtained.
- The corrosion rates of carbon steel in CO_2-saturated water were very high but did not change much with pressure from 40 to 80 bar.

ACKNOWLEDGMENTS

The authors would like to acknowledge the financial support from Ohio Coal Development Office (OCDO) for the Institute for Corrosion and Multiphase Technology at Ohio University.

REFERENCES

1. IPCC Special Report, “Carbon Dioxide Capture and Storage: Technical Summary” (2005), pp. 29
2. D.P. Connell, “Carbon Dioxide Capture Options for Large Point Sources in the Midwestern United States: An Assessment of Candidate Technologies,” Final Report, (South Park, PA: CONSOL Energy Inc. 2005)
3. J. Gale, and J. Davison, Energy (July-August 2004), p. 1319
4. H. Kruse, and M. Tekiela, Energy Conversion and Management (June 1996), p. 1013
5. S.H. Stevens, and J. Gale, Oil and Gas Journal (October 2000), p. 4
6. M. Seiersten, and K.O. Kongshaug, “Materials Selection for Capture, Compression, Transport and Injection of CO2”, in Carbon Dioxide Capture for Storage in Deep Geologic Formations, Vol. 2, D.C. Thomas and S.M. Benson Eds. (Elsevier Ltd. 2005), pp. 937
7. K.O. Kongshaug, and M. Seiersten, “Baseline Experiments for the Modelling of Corrosion at High CO_2 Pressure”, CORROSION/2004, paper no. 04630 (Houston, TX: NACE, 2004)
8. E.M. Russick, G.A. Poulter, C.L.J. Adkins, and N.R. Sorensen, The Journal of Supercritical Fluids, (January 1996), p. 43
9. W.A.Propp, T.E.Carleson, C.M.Wai, P.R.Taylor, K.W.Daehling, S.Huang, and M. Abdel-Latif, “Corrosion in Supercritical Fluids”, US Department of Energy report DE96014006, (Washington DC, 1996)
10. N. Spycher, K. Pruess, and J. E. King, Geochimica et Cosmochimica Acta (August 2003), p. 2619
11. M. Nordsveen, S. Nesic, R. Nyborg, and A. Stangeland, Corrosion (May 2003), p. 443
12. O. Redlich and J.N.S. Kwong, Chemical Reviews (February 1949), p. 233
13. J.M. Prausnitz, R.N. Lichtenthaller, and E.G. De Azedevo, “Molecular Thermodynamics of Fluid Phase Equilibria”, (New York, NY: Prentice Hall, 1986)
14. B. Brown, K.L. Lee, and S. Nesic, “Corrosion in Multiphase Flow Containing Small Amounts of H_2S”, CORROSION/2003, paper no. 03341, (Houston, TX: NACE, 2003)
15. W. Sun, “Kinetics of Iron Carbonate and Mixed Iron Carbonate/Sulfide Layer Formation in CO_2/H_2S Corrosion, (Ph.D. diss., Ohio University, 2006)
16. K-L J. Lee, A Mechanistic Modeling of CO_2 Corrosion of Mild Steel in the Presence of H_2S, (Ph.D. diss., Ohio University, 2004)
17. J. Greenberg and M. Tomson, Applied Geochemistry (March 1992), p. 185
18. ASTM Standard G 31, “Standard Practice for Laboratory Immersion Corrosion Testing of Metals,” in Annual Book of ASTM Standards, vol. 03. 02 (West Conshohocken, PA: ASTM International, 1994)
19. Y. Ji, X. Ji, X. Feng, C. Liu, L. Lu, and X. Lu, Chinese Journal of Chemical Engineering (March 2007), p. 439
20. H. Teng, and A. Yamasaki, Chemical Engineering Communications (November 2002), p. 1485
21. R. Wiebe, Chemical Reviews (December 1941), p. 475
22. C.R. Coan, and A.D. King, Jr., Journal of the American Chemical Society (April 1971), p. 1857
23. K.Y. Song, and R. Kobayashi, SPE Formation Evaluation (December 1987), p. 500
24. J.A. Briones, J.C. Mullins, M.C. Thies, and B.U. Kim, Fluid Phase Equilibria (October 1987), p. 235
25. M.B. King, A. Mubarak, J.D. Kim, and T.R. Bott, The Journal of Supercritical Fluids (December 1992), p. 296

26. A. Bamberger, G. Sieder, and G. Maurer, The Journal of Supercritical Fluids (April 2000), p. 97
27. S. Nesic, Corrosion Science (December 2007), p. 49
28. D.W. Shoesmith, P. Taylor, M.G. Bailey and D.G. Owen, Journal of the Electrochemical Society (May 1980), p. 1007

TABLE 1
ELEMENT ANALYSIS FOR THE X65 CARBON STEEL USED IN THE TESTS (WT %)

C	Mn	Si	P	S	Cr	Cu	Ni	Mo	Al
0.065	1.54	0.25	0.013	0.001	0.05	0.04	0.04	0.007	0.041

FIGURE 1 – The Test Autoclave Used for Corrosion Experiments

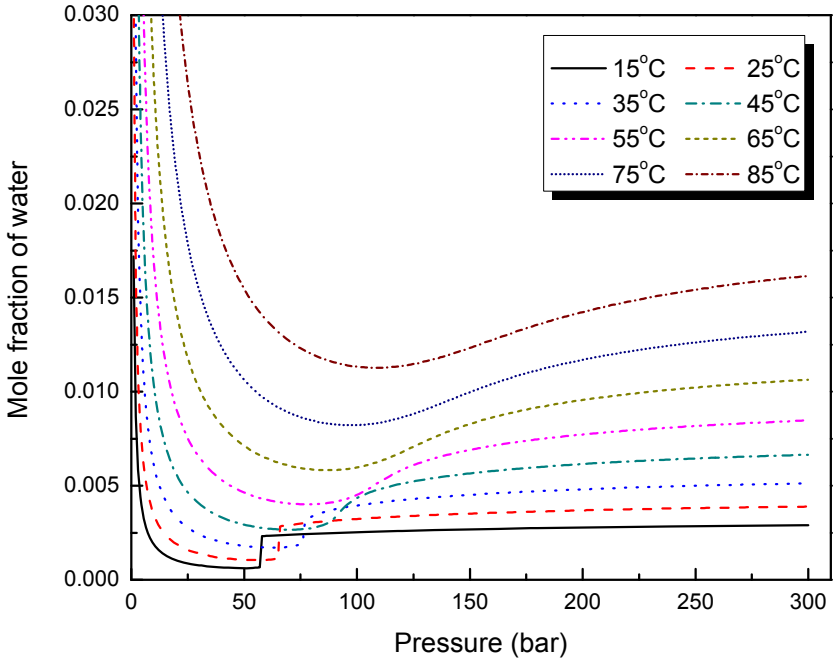

FIGURE 2 – Solubility of Water in CO_2 as Functions of Pressure and Temperature

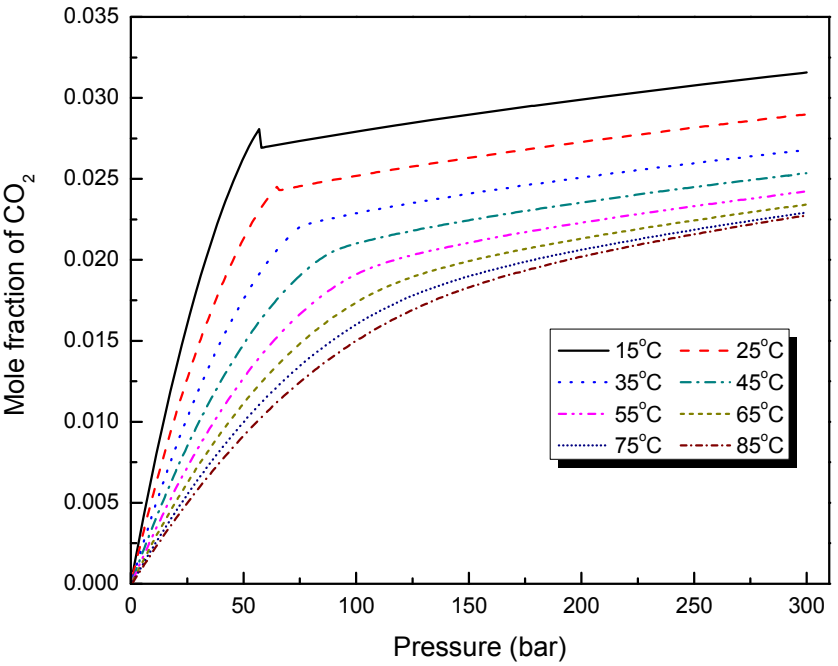

FIGURE 3 – Solubility of CO_2 in Water as Functions of Pressure and Temperature

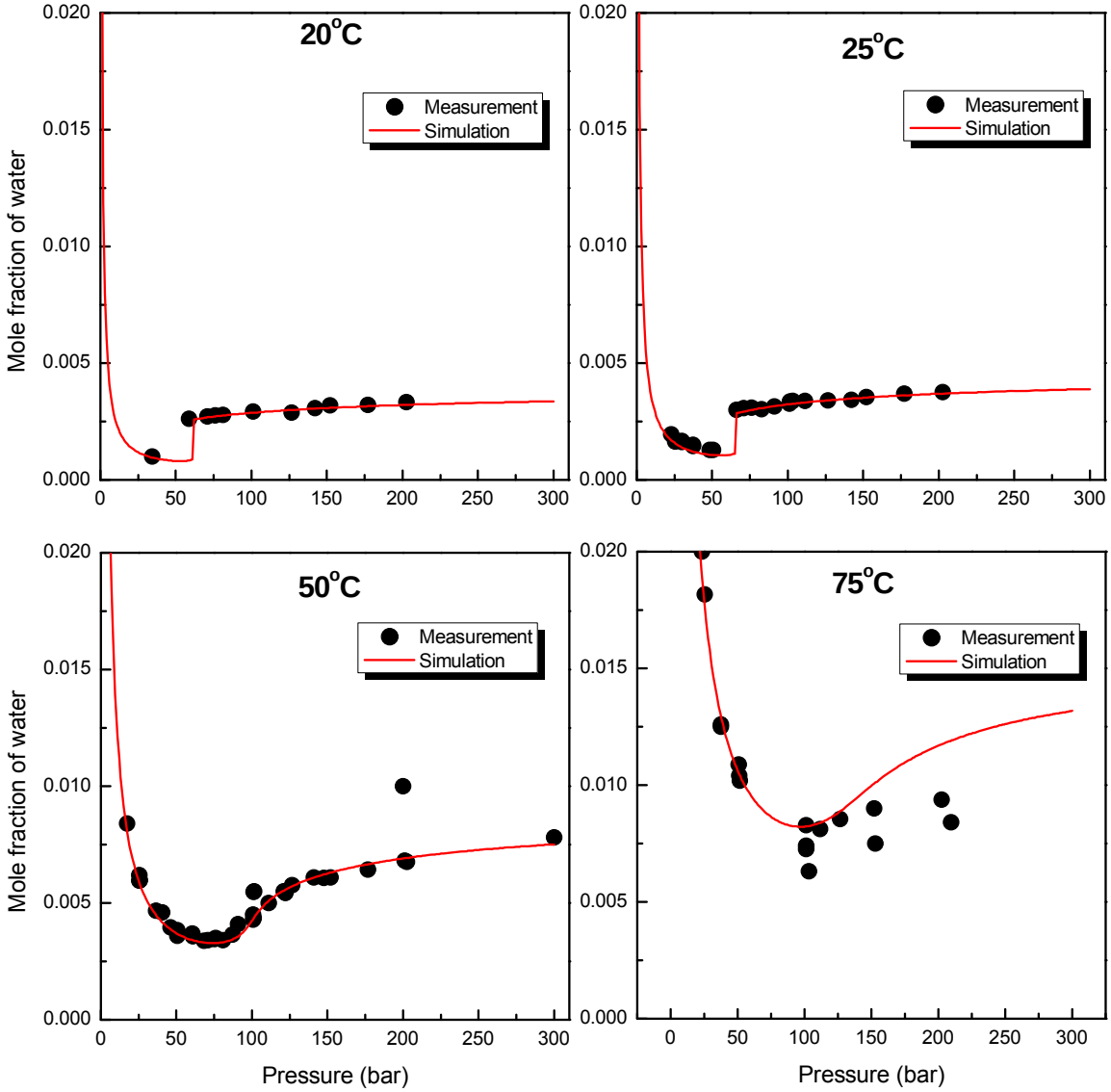

FIGURE 4 – Comparison between Experimental Data and Calculated Water Solubility in CO_2 at Various Pressures and Temperatures

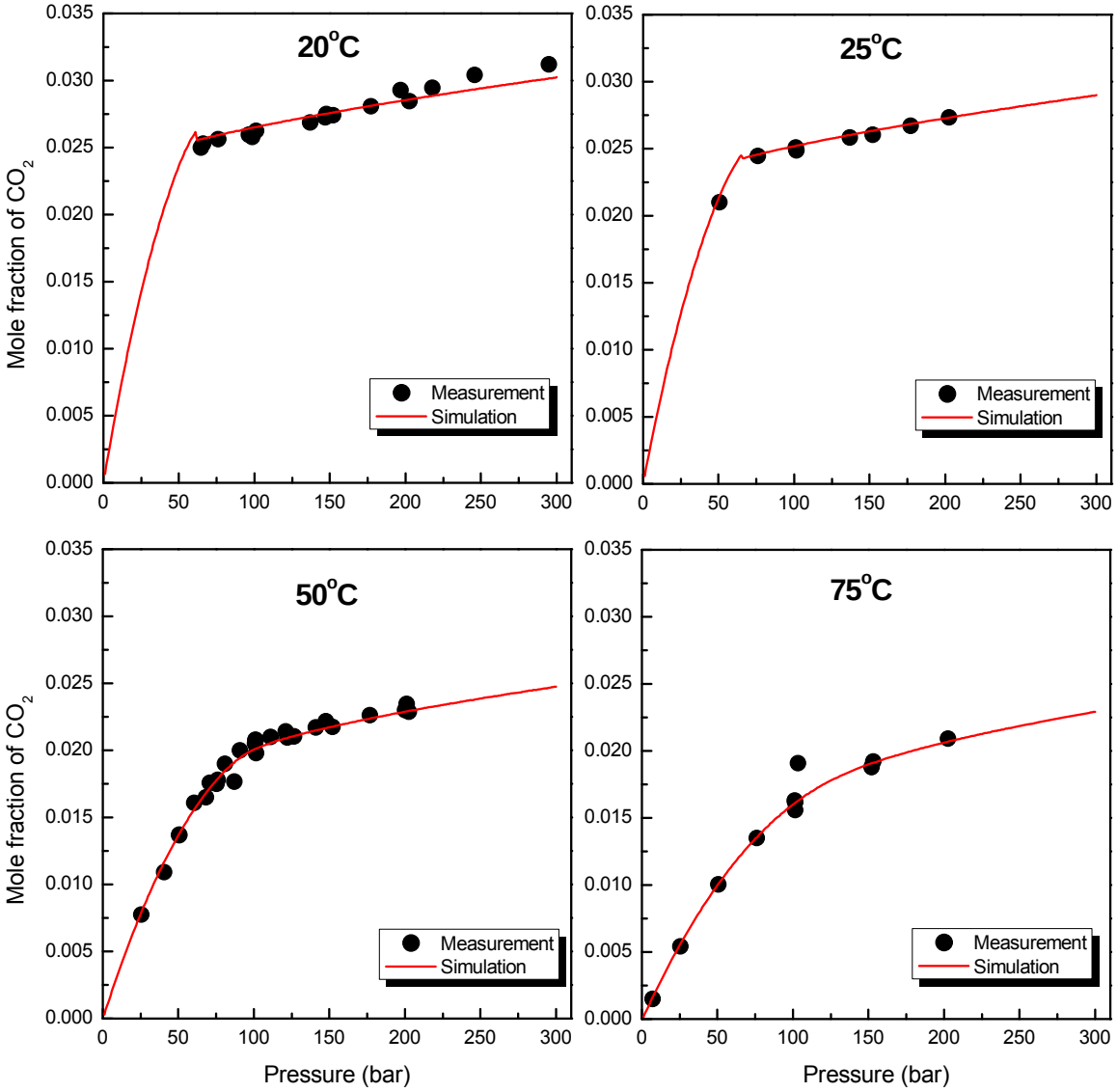

FIGURE 5 – Comparison between Experimental data and Calculated CO_2 Solubility in Water at Various Pressures and Temperatures

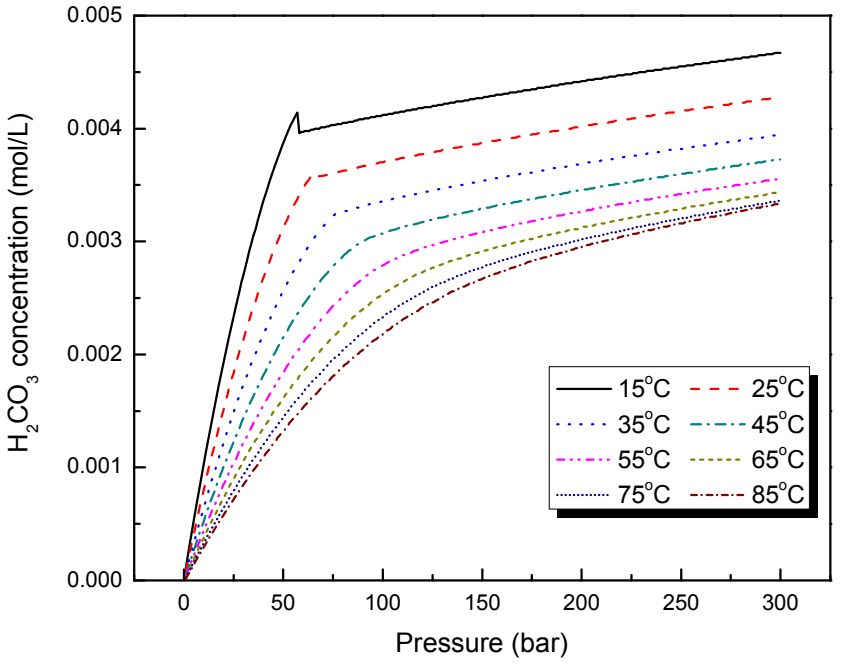

(a)

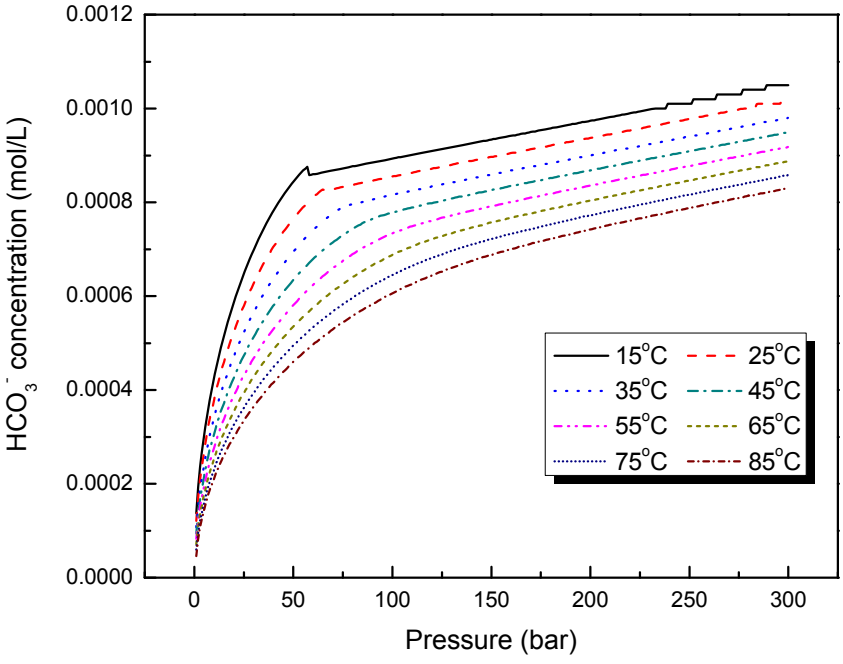

(b)

FIGURE 6 – Variations of (a) H_2CO_3 and (b) HCO_3^- Concentrations as Functions of Pressure and Temperature

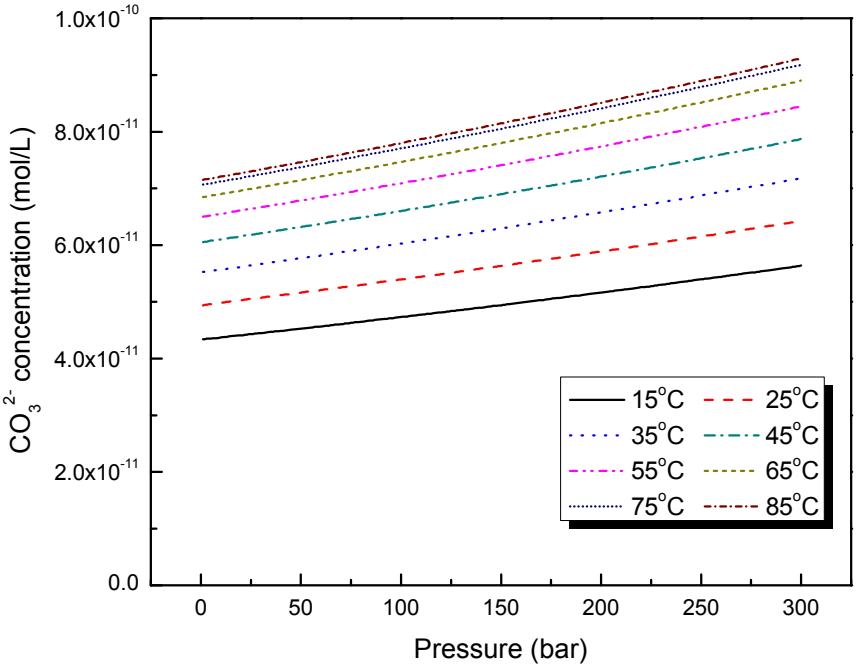

(a)

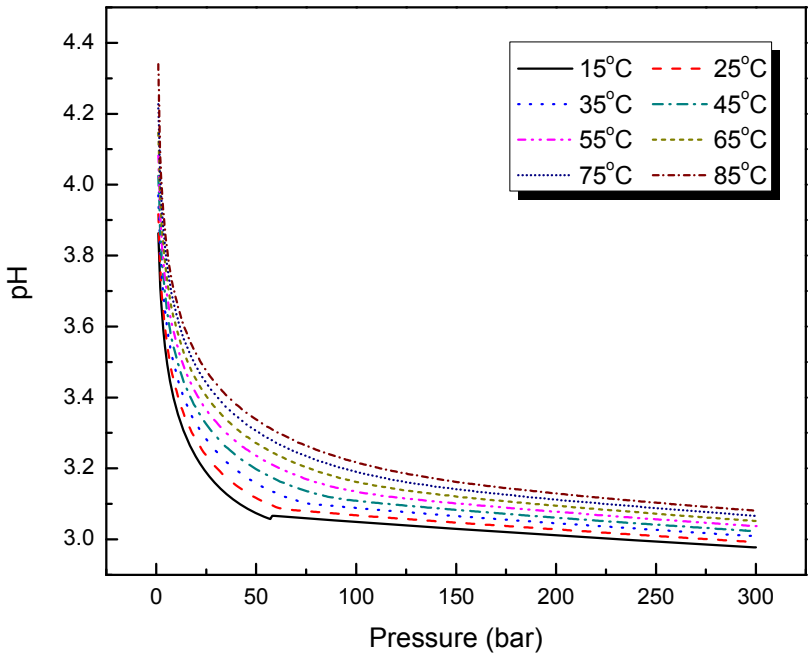

(b)

FIGURE 7 – Variations of (a) CO_3^{2-} Concentration and (b) pH as Functions of Pressure and Temperature

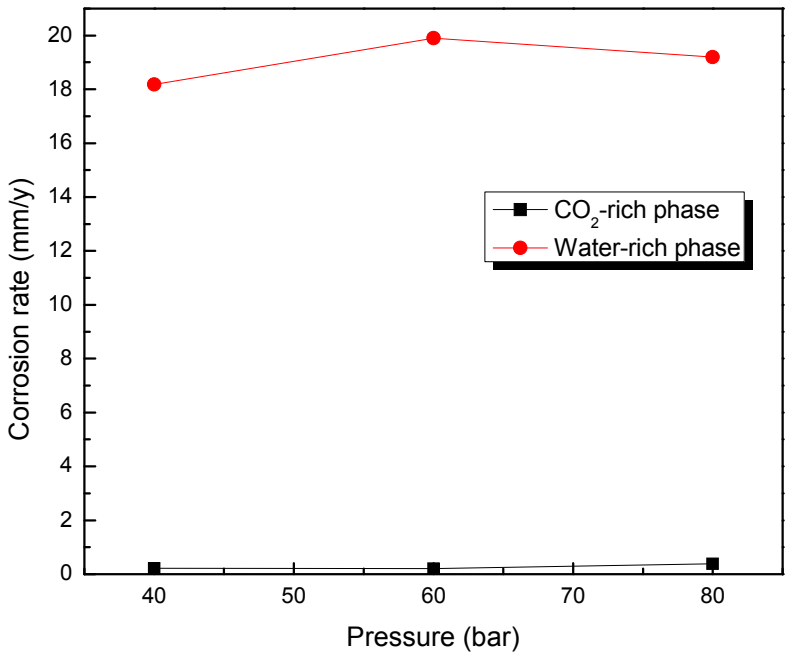

FIGURE 8 – Corrosion Rates in CO_2-Rich and Water-Rich Phases at 50°C as a Function of Pressure

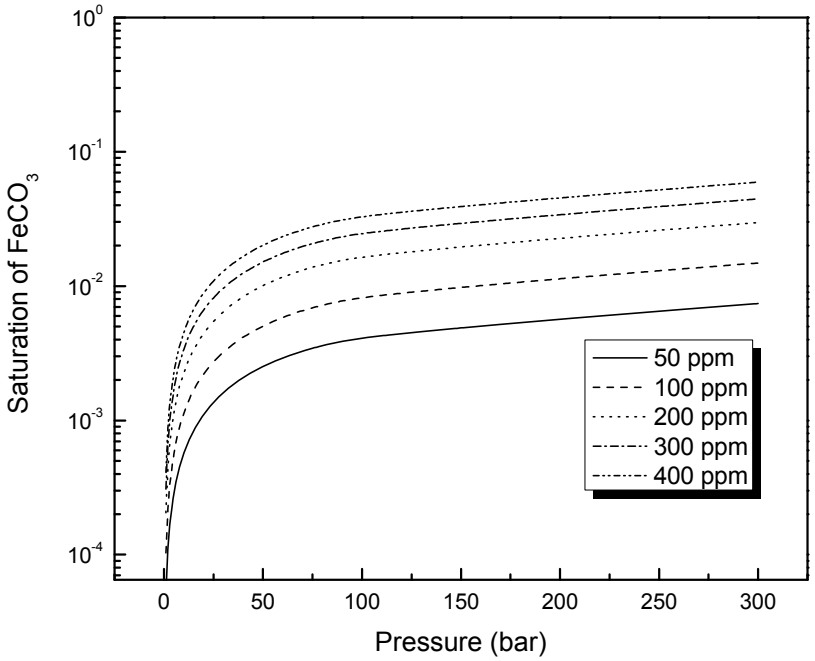

FIGURE 9 – Prediction of $FeCO_3$ Precipitation at Various Pressure and Fe^{2+} Concentration for T= 50°C, pH= 3

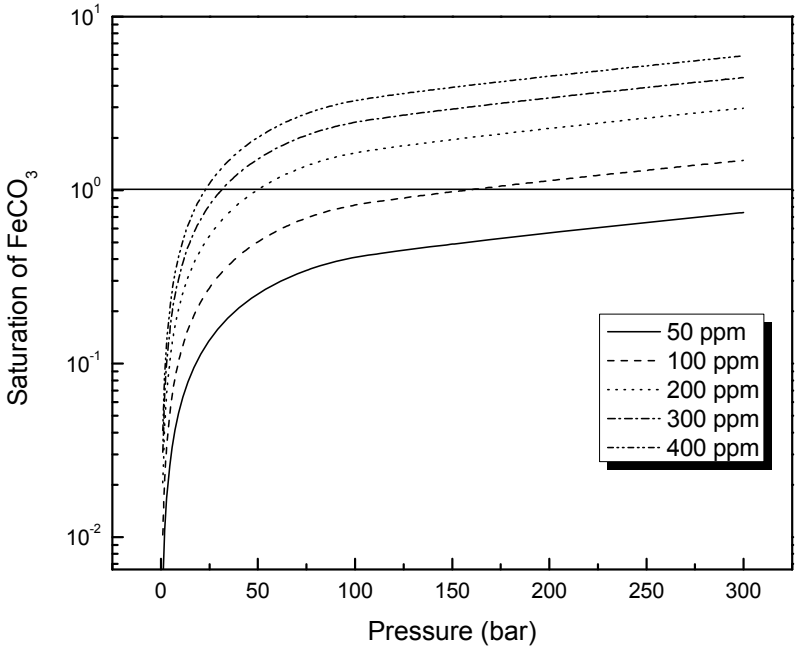

FIGURE 10 – Prediction of $FeCO_3$ Precipitation at Various Pressure and Fe^{2+} Concentration for T= 50°C, pH= 4

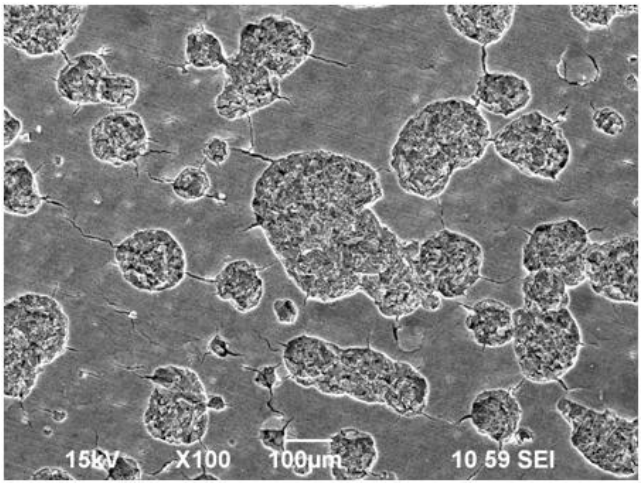

(a)

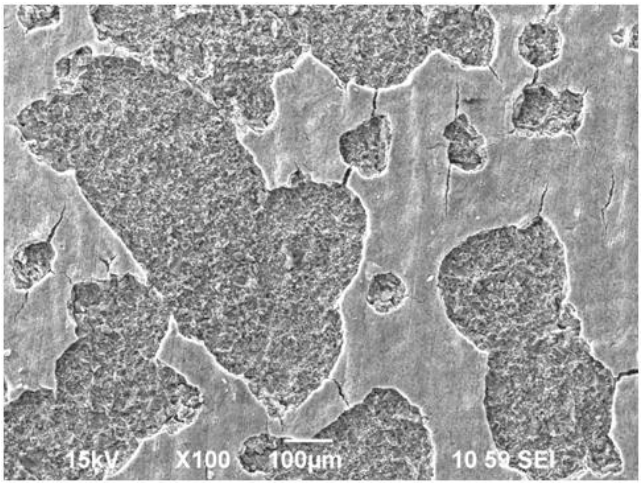

(b)

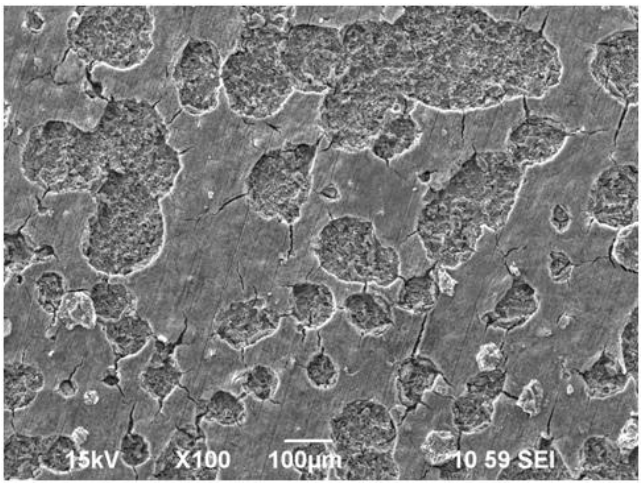

(c)

FIGURE 11 – SEM Images of the Corroded Surface of Samples Exposed in CO_2-Saturated Water with Different Pressures: (a) 40 bar, (b) 60 bar, and (c) 80 bar

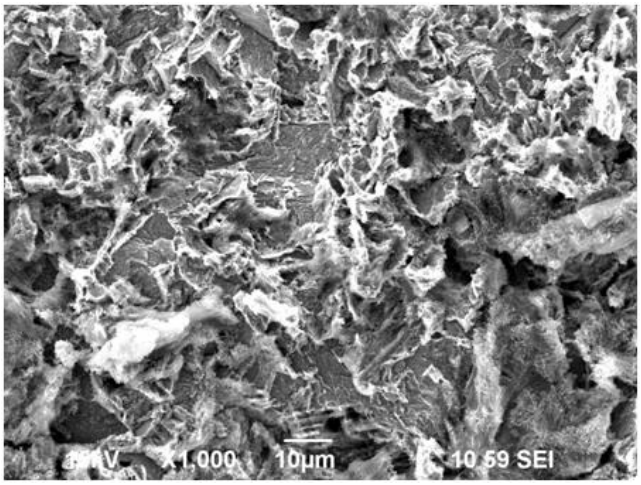

(a)

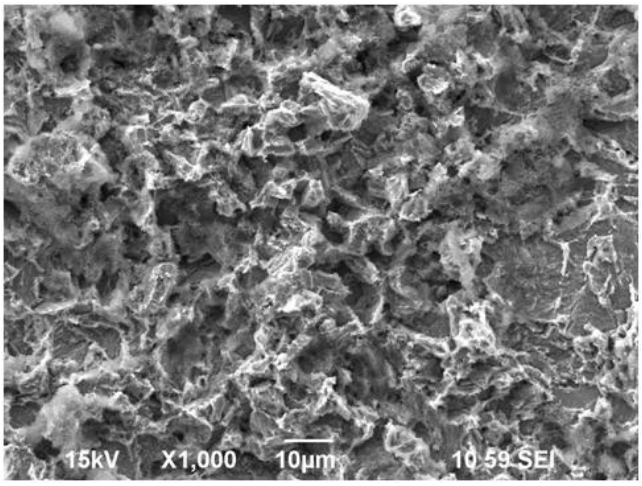

(b)

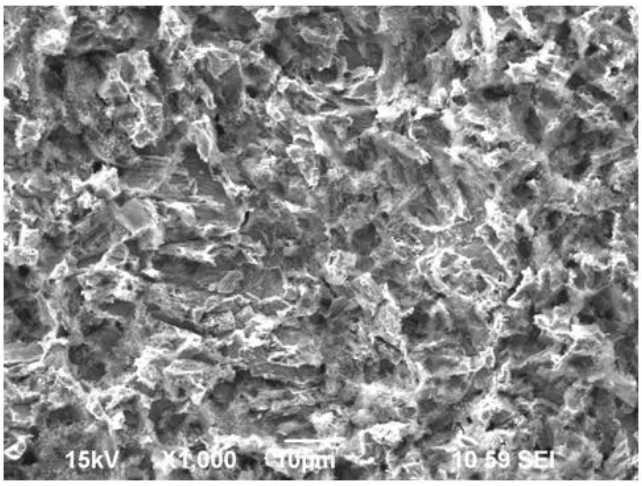

(c)

FIGURE 12 – SEM Images of the Corroded Surface of Samples Exposed in CO_2-Saturated Water with Different Pressures (After Cleaning): (a) 40 bar, (b) 60 bar, and (c) 80 bar